Characterization of Multimode Soliton Self-Frequency Shift

M. Zitelli, *Member, Optica,* M. Ferraro, *Member, Optica,* F. Mangini, and S. Wabnitz, *Member, Optica IEEE*

***Abstract*— Optical solitons in multimode fibers exhibit complex dynamics, and peculiar characteristics in terms of pulse duration and energy, which distinguish them from the single-mode counterpart. We propose a theory for Raman-induced soliton self-frequency shift in multimode fibers, that is compared against experimental data of 1-km multimode soliton propagation. Specific values of pulsewidth and energy are found, at which solitons show long-distance stability and better correspondence with the theory of self-frequency shift; those values depend on the input wavelength, but are not related to the duration of the input pulse. Raman delay is affected by a jitter, characterized by a Gaussian statistical distribution, whose standard deviation tends to stabilize to a constant value for increasing pulse energies.**

***Index Terms*—Fiber nonlinear optics, Optical solitons, Raman scattering.**

I. Introduction

The propagation of optical solitons in multimode (MM) fibers has been theoretically predicted over 40 years ago [1]. MM fiber solitons are a relatively accessible example of otherwise elusive objects such as spatiotemporal solitons or light bullets [2], where dispersion and diffraction are simultaneously balanced by nonlinearity and linear waveguiding. Since then, the field of MM fiber solitons has remained largely unexplored, especially when compared with their extensively investigated single-mode counterparts. Motivated by the potential use of MM fibers in spatial-division multiplexing (SDM) communications [3] and fiber lasers [4], experimental studies on MM fiber solitons have gained an increasingly renewed research attention over the past ten years [5-9].

The first evidence of soliton self-frequency shift (SSFS) was reported by Mitschke and Mollenauer in [10], by using sub-picosecond pulses propagating in a single-mode, polarization preserving fiber span of 390 m. Those experiments have shown that the soliton pulse was affected by a spectral red-shift induced by Raman nonlinearity. This SSFS could be easily distinguished from other dissipative effects induced by the stimulated Raman scattering (SRS), because of its graduality: the spectral shift is continuous for solitons, and does not break-up the spectrum into multiple lobes. A first theory for the SSFS was proposed by Gordon in [11] for single-mode optical fibers: from the lossless nonlinear Schrödinger equation including the Kerr and Raman exact models, a differential equation for the frequency shift was obtained, starting from the Raman gain spectrum $G(\nu)$. The theory assumed the soliton to maintain a constant temporal duration. In [12], Grudinin et al. reported the first observation of a soliton produced by SRS in 50 m of parabolic graded-index fiber (GRIN): an ultra-short pulse with 90 fs duration, at 1650 nm, was generated from a 150 ps pump pulse at 1064 nm, with 600 kW peak power. A more complete theory for the Raman frequency shift in single-mode fibers, in the presence of losses, dispersive effects, and considering a Raman nonlinear term described by a finite response time T_R, was developed in [13]. However, a more accurate theory describing chirped pulse evolution in single-mode fibers, including losses and high-order dispersion, was introduced much later [14] based on the moment method: a set of differential equations was found, describing the adiabatic evolution of the pulse energy, delay, frequency shift, duration and chirp. The adiabatic approach was also introduced to describe the interaction between Raman soliton and group velocity matched pulses [15].

Besides the accuracy demonstrated by the above theories in single-mode pulse transmission, no comparison was carried out, to the best of our knowledge, with experiments on multimode solitons in GRIN fibers. Here, the pulsewidth evolution is affected by modal dispersion, losses and inter-modal nonlinear interactions: as a result, the soliton behavior is somewhat different from the single-mode counterpart [5], and it must be described in terms of the walk-off theory [16]. Raman-induced SSFS still holds, but it is strongly affected by the multimode soliton evolution; hence, a quantitative comparison between theoretical predictions and experimental results for multimode soliton propagation should be carried out.

This comparison is precisely the scope of our work: we found a good agreement between theory and experimental results, providing that: (i) the propagating soliton pulse has a specific energy, which depends on the input wavelength; (ii) an effective waist for the multimode soliton beam is used in the

This work was supported by: the European Research Council (ERC) under the European Union's Horizon 2020 research and innovation programme (No. 874596, No. 740355, No. 101081871). The Italian Ministry of University and Research (R18SPB8227). Sapienza University of Rome (RG12117A84DA7437, AR22117A7B01A2EB).

M. Zitelli, M. Ferraro, F. Mangini, and S. Wabnitz are with the Department of Information Engineering, Electronics and Telecommunications (DIET), Sapienza University of Rome, Via Eudossiana 18, 00184 Rome, Italy (e-mail: mario.zitelli@uniroma1.it).

S. Wabnitz is also with CNR-INO, Istituto Nazionale di Ottica, Via Campi Flegrei 34, 80078 Pozzuoli (NA), Italy.

theory. Our paper is organized as follows: in Section 2, multimode soliton pulsewidth evolution will be studied numerically and experimentally, in order to find out if there are any substantial differences with respect to the single-mode soliton case. In Section 3, a theory for the SSFS and for the Raman delay of multimode solitons will be introduced, and tested against both experimental and numerical results.

II. Multimode Soliton Pulsewidth

Before moving to the theory for multimode SSFS, it is necessary to point out the differences between single-mode and multimode solitons. In the former case, the pulse adjusts its duration according to the energy coupled at the input, and to the chromatic dispersion of the fiber; in the latter case, the so-called walk-off soliton forms at a specific optimal energy, and it takes an initial pulsewidth, which is only dependent on the fiber's dispersion parameters, and it remains independent on the duration of the pulse coupled at the fiber input [16]. Such peculiarity restricts the validity of the SSFS theory to a limited pulse energy interval, as it will be shown in Section 3.

A. Pulsewidth Invariance in Multimode Solitons. Simulations

Numerical simulations use a coupled-mode equations model derived from [17-20]; right-side terms of Eq. 2.1 describe: modal dispersion, four orders of chromatic dispersion, wavelength-dependent losses, random modal coupling (with coefficient q_{mp}, limited to degenerate modes), nonlinear Kerr and Raman terms, respectively. The Q_{plmn} are cross-terms corresponding to the inverse of effective modal areas, providing appropriate weights to inter-modal four-wave mixing (IM-FWM) and Raman scattering (IM-SRS) terms. The Raman term contributes with a fraction $f_R = 0.18$; the expression $h * (A_m A_n^*)$ denotes for time convolution with the Raman response function $h(t)$, with typical time constants of 12.2 and 32 fs [21,22]. Fiber parameters at wavelength λ =1450 nm are: $\beta_2 = -16.27$ ps^2/km, $\beta_3 = 0.12$ ps^3/km, $\alpha = 1.38 \times 10^{-4}$ m^{-1}, $n_2 = 2.6 \times 10^{-20}$ m^2/W. The modal distribution of power at the fiber input was calculated by field superposition integrals.

$$\begin{aligned}\frac{\partial A_p(z,t)}{\partial z} = {} & i\left(\beta_0^{(p)} - \beta_0\right)A_p - \left(\beta_1^{(p)} - \beta_1\right)\frac{\partial A_p}{\partial t} \\ & + i\sum_{n=2}^{4}\frac{\beta_n^{(p)}}{n!}\left(i\frac{\partial}{\partial t}\right)^n A_p - \frac{\alpha_p(\lambda)}{2}A_p \\ & + i\sum_m q_{mp}A_m + i\frac{n_2\omega_0}{c}\left(1 + \frac{i}{\omega_0}\frac{\partial}{\partial t}\right) \\ & \cdot \sum_{l,m,n} Q_{plmn}\{(1-f_R)A_l A_m A_n^* \\ & + f_R A_l[h * (A_m A_n^*)]\}\end{aligned} \quad . \qquad (2.1)$$

Fig. 1 (a) reports the simulated pulsewidth vs. input energy for a pulse propagating over 1 km of GRIN fiber, with input parameters: 1450 nm wavelength, 42 μm beam diameter, 60 fs or 300 fs pulsewidth. Power is distributed with fractions 0.497, 0.309, 0.193 among the first Laguerre-Gauss modes with axial symmetry, i.e., with radial/azimuthal indexes $(p,m) = (0,0), (1,0), (2,0)$. Non-axial mode power is neglected at the fiber input.

The soliton pulsewidth at short distances (a few meters), immediately after the soliton formation, scales in agreement with the single-mode soliton formula [5]

$$T_0 = \frac{\lambda|\beta_2(\lambda)|w_e^2}{n_2 E_s} \quad , \qquad (2.2)$$

where E_s is the soliton energy, w_e is an effective modal waist, and soliton duration $T_0 = T_{FWHM}/1.763$, with T_{FWHM} the pulsewidth (full-width half-maximum); both pulses with input pulsewidths of either 60 fs or 300 fs appear to generate, after a few meters, a pulse with nearly the same pulsewidth, for any values of the input energy.

In order to apply Eq. 2.2 to MM solitons, an effective beam waist w_e must be used, in place of the single-mode waist; from the theory of self-imaging in GRIN fibers [23-26], the modal effective area oscillates with distance z according to the law $cos^2(\pi\, z/z_p) + C^2\, sin^2(\pi\, z/z_p)$, with $z_p = \pi r_c/\sqrt{2\Delta}$ the self-imaging period, and $C \approx \lambda\, z_p/(\pi^2 n_0 w_{in}^2)$ the oscillation amplitude, being w_{in} the input beam waist, n_0 and r_c the core index and radius, respectively, and Δ the relative index difference between core and cladding. The mean effective area is $A_{eff} = \pi w_{in}^2\,(1 + C^2)/2$, hence, the effective beam waist is

$$w_e = w_{in}\sqrt{\frac{1+C^2}{2}} \quad . \qquad (2.3)$$

Eq. 2.3 over-estimates the effective waist of a multimode soliton at large distances, because most of the soliton energy tends to flow into the fundamental mode, whose waist is $w_0 = \sqrt{\lambda r_c/\left(\pi n_0\sqrt{2\Delta}\right)}$. Hence, the effective waist should be calculated by accounting for the evolution of the power distribution within modes; its value gradually decreases from what predicted by Eq. 2.3 down to w_0.

When the pulsewidth at large distances is observed (e.g., at 1 km), a common minimum value of 220 fs, at the optimal input energy of 1 nJ, is obtained for both input pulsewidths of 60 and 300 fs. Hence, only a single soliton state is formed at large distances, with a specific soliton duration and energy, independently of the input pulse duration.

For such optimal pulse energy, the soliton pulsewidth increases with distance because of the Raman-induced SSFS, which is responsible for increasing the soliton wavelength, hence of the absolute value of the chromatic dispersion experienced by the red-shifted soliton. In the example of Fig. 1, at 1 nJ input energy the soliton wavelength grows from 1450 to 1548 nJ after 1 km distance. Correspondingly, the soliton pulse increases its time duration from 205 fs at 20 m distance, up to 220 fs at 1 km, in order to conserve the soliton condition of Eq. 2.2.

This article has been accepted for publication in IEEE/OSA Journal of Lightwave Technology. This is the author's version which has not been fully edited and content may change prior to final publication. Citation information: DOI 10.1109/JLT.2022.3205846

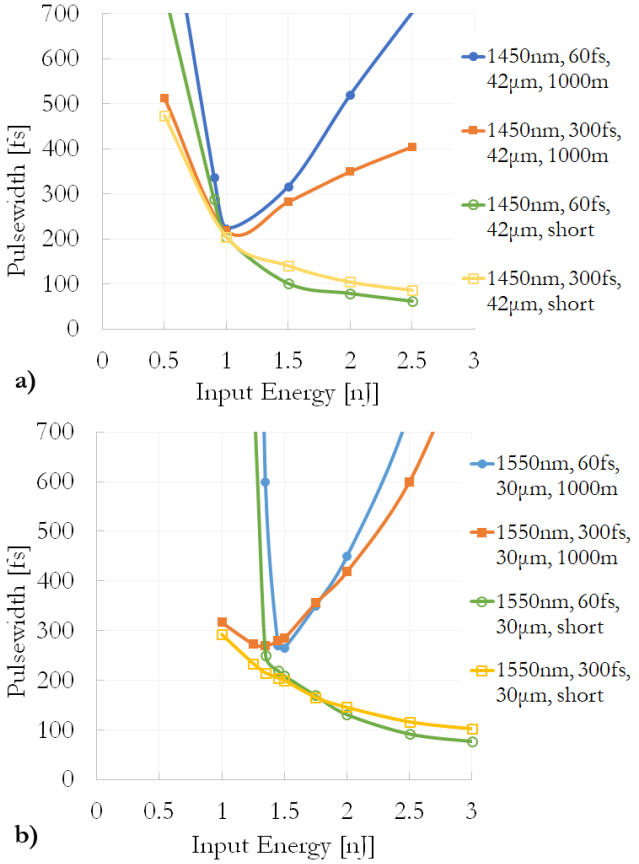

Fig. 1 – Simulated pulsewidth vs. input energy for a pulse propagating over 1 km of GRIN fiber; input parameters are: (a) 1450 nm (b) 1550 nm wavelength, 42 μm beam diameter, 60 fs or 300 fs pulsewidth.

Fig. 1 (b) shows that similar results are obtained with the following input parameters: 1550 nm wavelength, 30 μm beam diameter, 60 fs or 300 fs pulsewidth. The input power is distributed with fraction 0.519, 0.303, and 0.177 among the first 3 axial modes. Hence, a longer wavelength and a smaller beam diameter are used with respect to the case in Fig. 1 (a). Still, an optimal input energy of 1.5 nJ is found at 1 km of distance, providing same output pulsewidth of 270 fs for both input conditions of 60 fs and 300 fs; at 20 m distance, a common pulsewidth of 215 fs is also obtained. The optimal input energy may vary by a few percents in the two cases of 60 fs and 300 fs input, for two reasons: first, because the 60 fs pulse appears generating a larger amount of dispersive waves during the soliton formation process; second, because for large Raman-induced wavelength shifts, fiber losses start to affect the pulse duration. The soliton pulsewidth at the optimal energy increases with distance, because the Raman SSFS is responsible for a wavelength increase, from 1550 nm at the fiber input up to 1650 (1740) nm after 1 km, for input pulsewidth of 60 (300) fs.

By comparing Figs. 1 (a) with Fig.1 (b), we observe that the optimal input energy for long-distance soliton formation increases with wavelength, from 1.0 nJ at 1450 nm up to 1.5 nJ at 1550 nm. The soliton pulsewidth also increases with wavelength, from 205 fs to 215 fs at short distances, and from 220 fs to 270 fs at 1 km.

The pulsewidth invariance of the forming soliton with respect to the input pulse duration was previously explained in terms of the walk-off soliton theory [16,27]. This involves introducing: (i) the mean modal walk-off length of the forming soliton $L_W = T_0/\overline{\Delta\beta_1}$, where $\overline{\Delta\beta_1}$ the mean group velocity difference between modes (ps/km); (ii) the pulse nonlinearity length $L_{NL} = \lambda T_0 w_e^2/(n_2 E_s)$; (iii) and the dispersion length $L_D = T_0^2/|\beta_2|$. When nonlinearity acts over distances shorter than those associated with random mode coupling and birefringence, i.e., for $L_{NL} < L_{cm}, L_{cp}$, a multimode soliton involving non-degenerate modes may form after a few meters, provided that both the dispersion and nonlinearity lengths are comparable with the fiber walk-off length, i.e., $L_D = L_{NL} = const \cdot L_W$, being *const* an adjustment constant close to unity, which depends on the input beam coupling conditions. After hundreds of meters, the spatiotemporal soliton is eventually attracted into an effectively single-mode soliton [28]. Based on the above considerations, we may find the condition to be respected by the soliton pulsewidth at the point of its initial formation

$$T_s(\lambda) = const \cdot 1.763 \frac{|\beta_2(\lambda)|}{\overline{\Delta\beta_1}(\lambda)} \quad , \tag{2.4}$$

which explains why two pulses with different input pulsewidths, but same wavelength, generate the same soliton at the fiber output. Pulses also share the same soliton energy, which is associated with the common pulse duration T_0 by Eq. 2.2. A different amount of dispersive wave is eventually generated by the two input pulses, which explains the small difference among the input energies.

Only marginal dependence of the soliton pulsewidth from the input beam diameter (the coupling conditions) was found, when changing its value from 30 μm to 42 μm. On the other hand, we noticed an increase in the optimal energy for long-distance soliton formation, that increases with the square of the soliton effective waist, in agreement with Eq. 2.2.

B. Experimental Investigation of Pulsewidth Evolution

In order to verify experimentally the Raman-induced SSFS, and the wavelength dependence of the MM soliton pulsewidth, a femtosecond Yb laser is used to feed an optical parametric amplifier (OPA), generating 60, 70, and 60 fs pulses at 1450, 1550, 1650 nm, respectively, with 100 kHz repetition rate. Pulses are injected into an 830 m span of GRIN fiber, with $1/e^2$ input diameter of approximately 30 μm (15 μm beam waist, M^2 = 1.3), and in a separate experiment into a 1 km span, with input beam diameter of 42 μm. The GRIN fiber is a commercial OM4 type fiber, 50/125 μm core/cladding diameter, cladding index n_{clad} = 1.445 at 1450 nm, and relative index difference Δ = 0.0103. The laser pulse input energy is controlled by means of an external attenuator, and varied between 0.1 nJ and 6 nJ. At the fiber output, a micro-lens focuses the near-field on an InGaAs camera (Hamamatsu C12741-03); a second lens focuses the beam into a real-time multiple octave spectrum analyzer (Fastlite Mozza) with a spectral detection range of 1100-5000 nm. The output pulse temporal shape is inspected by a fast photodiode (Alphalas UPD-35-IR2-D) and a real-time

oscilloscope (Teledyne Lecroy WavePro 804HD) with 30 ps overall response time, and an intensity autocorrelator (APE pulseCheck 50) with femtosecond resolution. Input and output power are measured by a power meter with μW resolution.

Fig. 2 provides the measured pulsewidth, after 6 m or after 830 m of GRIN fiber, respectively, vs. the soliton energy. By comparing the output spectra and power, we extracted the energy of the emerging soliton pulse. Input wavelength and pulsewidth used in this first experiment are: 1450 nm and 60 fs, 1550 nm and 70 fs, 1650 nm and 60 fs, respectively; the input beam diameter is approximately 30 μm. As observed in our simulations, we experimentally confirmed the existence of an optimal pulse energy that provides a minimum long-distance pulsewidth. Whereas the soliton energy increases with wavelength (1.0, 1.5, 2.2 nJ at 1450, 1550, 1650 nm, respectively). Such an effect is not visible at short distances (6 m), where the pulsewidth of the forming soliton agrees well with the theory of Eq. 2.2, provided an effective waist $w_e = 9.5$ μm is used, close to the fundamental mode waist of 7.8 μm. The only visible difference from the short-distance pulsewidth, with respect to the theory, is a small local increase of the pulse duration, immediately above the value of optimal energy for long-distance soliton formation.

In Fig.2, theoretical curves at 1550 nm, 6 m and 830 m distance, respectively, are calculated from Eqs. 3.4 (see next section) and Eq. 2.2, and account for the Raman-induced red-shift, wavelength-dependent dispersion and linear fiber losses. At relatively short distances, the theory provides a fair agreement with the experimental data at all the tested input energies. Whereas at long distances, the wavelength-dependent losses are partially responsible, together with the Raman-induced wavelength red-shift, for the output pulsewidth increase which is observed at energies above its optimal value; the theoretical curve at long distances does not correctly reproduce the experimental data. A possible reason for this discrepancy is the presence of linear random mode coupling (RMC), which is responsible for power scrambling between degenerate modes, and may affect the experimental data by degrading the soliton stability at large distances. Simulations performed with strong random modal coupling between degenerate mode groups (not shown), confirm that RMC can affect both the pulse duration and the soliton formation. The theory which is derived for single-mode solitons, although using an effective modal waist, wavelength-dependent dispersion and losses, does not account for the presence of random mode coupling; hence it does not appear to be suitable for predicting the values of the long-distance multimode soliton pulsewidth, especially at pulse energies which do not correspond to the minimum pulsewidth.

On the other hand, the walk-off soliton theory of Eq. 2.3 is able to predict well the pulsewidth of the MM soliton that is formed at short distances. Starting from the measured soliton wavelengths of 1487, 1586, 1672 nm at 6 m of distance, with the optimal energies of 1.0, 1.5, 2.2 nJ, for input wavelength 1450, 1550, 1650 nm, respectively, using the GRIN fiber dispersion curves, and choosing an adjustment constant $const = 1.0$, the calculated solitons pulsewidth are 112, 158, 198 fs, respectively. The corresponding three points are indicated by red x-crosses in Fig. 2, and show excellent agreement with the experimental data. From Eq. 2.3 and Fig. 2, we understand that only a single point, for each experimental curve at short distances, obtained at the optimal energy, can be associated with a stable MM soliton, which eventually leads to a minimum pulsewidth at long distances.

In all of the three cases of 1450, 1550, 1650 nm input wavelength, a strong Raman-induced SSFS at 830 m affects the pulse propagation (not shown); the pulse wavelength may reach 1950 nm at 4 nJ of energy, for all input wavelengths. The next section will describe this effect in detail, by introducing the differential equations that are capable to predict the MM SSFS at the optimal soliton energy.

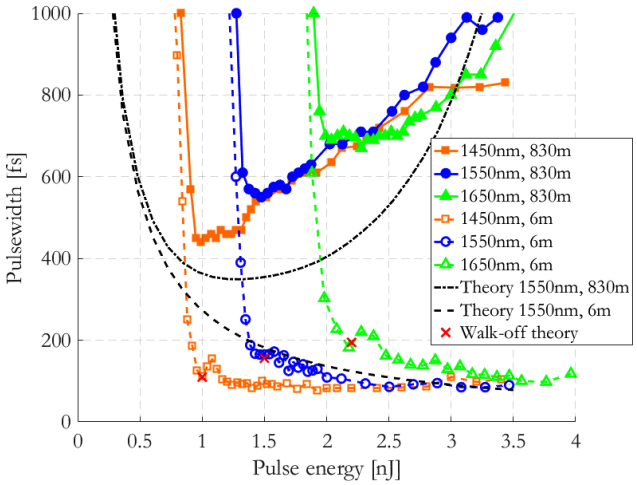

Fig. 2 – Experimental pulsewidth vs. soliton energy for a pulse propagating over 6 m or 830 m of GRIN fiber. Input parameters are: 1450 nm and 60 fs, 1550 nm and 70 fs, 1650 nm and 60 fs; 30 μm beam diameter. Theoretical curves are calculated from Eqs. 3.4 and 2.2. Red x-crosses come from Eq. 2.4.

III. MULTIMODE SSFS

A. *Theory and Experiment*

In order to test the theory of SSFS in the regime of long-distance MM soliton propagation, experiments were repeated over 1 km of parabolic GRIN fiber.

Fig. 3 shows the measured photodiode traces (top), output spectra (center) and beam near field (bottom), after 1 km of GRIN fiber. The following input pulse parameters were used: center wavelength at 1450 nm, pulse duration of 60 fs, and 42 μm beam diameter. Figure 3 illustrates the results for two cases of input energy: (a) 0.65 nJ, corresponding to the quasi-linear propagation regime, that is, immediately preceding the soliton formation, and (b) 2.57 nJ, corresponding to a well-formed soliton. By comparing the measured output power with the spectrum integration, we found that the optical soliton contains nearly 45% of the input energy. The remaining amount concurs to the formation of dispersive waves, whose presence is visible in the photodiode trace of case (b) as a broadened nanosecond pulse preceding the narrow soliton, and in the spectrum as an unshifted lobe, corresponding to the input pulse residue after soliton formation. Hence, 2.57 nJ of input energy corresponds approximately to the optimal energy value for soliton formation, that was found in the numerical simulations of Fig.

1, where the residual energy is limited to less than 10%. The difference in residual dispersive wave energy amount between simulations and experiments could be ascribed to the fact that, in experiments, the fiber is wrapped in a spool.

By comparing the near-field in the linear and in the soliton regime, one may clearly see the beam condensation process which is accompanying soliton formation. The beam waist was measured from the image root-mean-square, according to the standard ISO11146; in the experiment of Fig. 3, the output beam waist in the linear regime is 22.6 μm, while it reduces down to 16.1 μm at the input energy leading to soliton formation.

In the spectrum of Fig. 3(b) we can see the characteristic sech-shaped lobe of a soliton, which experiences wavelength red-shift by SSFS, and separates from the unshifted residual spectrum.

Previous works [28,29] have pointed out how the multimode soliton formation process causes an initial wavelength increase for the lower-order modes, and a decrease for the higher-order ones, in order to equalize the respective modal velocities and obtain temporal trapping. IM-SRS is responsible for a power transfer from the shorter wavelength modes to the longer wavelength ones, hence accelerating the promotion of the fundamental mode and, at the same time, causing SSFS.

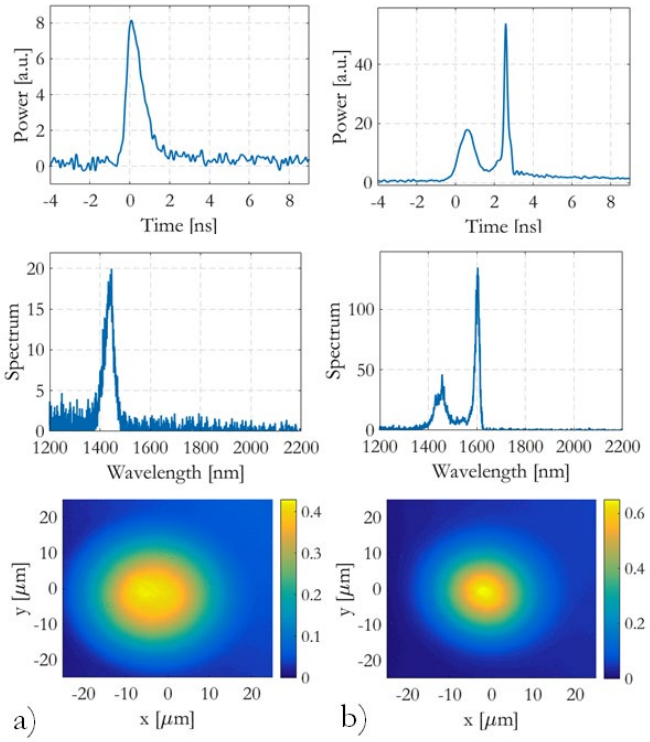

Fig. 3 – Experimental fast photodiode trace (top), spectrum (center), and beam near field (bottom) after 1 km of GRIN fiber, for input energy of (a) 0.65 nJ, and (b) 2.57 nJ.

Fig. 4 reports the measured Raman-induced wavelength shift after 1 km of GRIN fiber, for an input pulse with 1450 nm wavelength, 42 μm diameter, and 60 fs pulsewidth. Blue and green dots are experimental and numerical data, respectively, showing good agreement. The soliton energy which is reported on the *x*-axis was estimated in the experiment to reach 45% of the input energy: this value was extracted from the measured output spectra, by comparing the soliton with the dispersive spectral lobes, and referring to the measured output power. Whereas in numerical simulations, nearly all the input power (90-95%) was captured by the output soliton. A good agreement between experimental and numerical data was found, when accounting for energy loss via the emission of dispersive waves; at the optimal soliton energy of 1 nJ, its wavelength has shifted from 1450 nm to 1530 nm.

A theoretical description of the Raman-induced soliton self-frequency shift in MM fibers starts from the single-mode formula for the wavelength shift (obtained by neglecting fiber loss) of a soliton with fixed duration T_0 [11,13,14,30]

$$\Delta\lambda = 4\lambda^2|\beta_2|T_R z/(15\pi c T_0^4) \quad , \tag{3.1}$$

where $T_R = 3$ fs is the response time of the Raman nonlinearity [5]. Expression 3.1 is suitable for soliton pulsewidth much longer than 10 fs [22], but it must be re-formulated in differential terms when dealing with losses, and relatively fast changes over distance z of dispersion, pulsewidth and wavelength. In order to apply Eq. 3.1 to MM solitons, an effective beam waist w_e must be used, in place of the single-mode waist. By combining Eqs. 3.1 and 2.2, we obtain

$$\frac{d\Delta\lambda}{dz} = \frac{4T_R}{15\pi c\lambda^2(z)|\beta_2(z)|^3}\left(\frac{n_2 E_s}{w_e^2}\right)^4 . \tag{3.2}$$

The chromatic dispersion of the fiber changes with wavelength (and distance) according to

$$\beta_2(z) = -\frac{\lambda^2(z)}{2\pi c}D(\lambda) = -\frac{\lambda^2(z)}{2\pi c}\{D(\lambda_0) + S[\lambda(z) - \lambda_0]\}, \tag{3.3}$$

where D and S are the second and third-order dispersion terms expressed in s/m^2 and s/m^3, respectively, and $\lambda(z)$ the soliton wavelength. The model can be further improved by considering that the wavelength-dependent fiber losses $\alpha(\lambda)$ decrease the soliton energy, so that the soliton energy scales as $dE_s/dz = -\alpha(\lambda)E_s$. By replacing Eq. 3.3 into 3.2, we finally obtain

$$\frac{d\Delta\lambda}{dz} = \frac{2T_R}{15\lambda^8(z)D^3(\lambda)}\left[\frac{2\sqrt{\pi c}n_2 E_s(z)}{w_e^2}\right]^4 . \tag{3.4}$$

According to Eq. 3.4, the rate of SSFS induced by Raman nonlinearity decreases with the 8-th power of wavelength; the rate becomes negligible for $\lambda > 2.2$ μm.

The red curve in Fig. 4 is plotted by integrating Eq. 3.4, and including the wavelength dependence of the fiber dispersion and loss, with $D(\lambda_0) = 14.8$ ps/nm/km and $\alpha(\lambda_0) = 1.38 \times 10^{-4}$ m^{-1} at the input wavelength $\lambda_0 = 1450$ nm, and $S = 0.073$ ps/nm^2/km. For an input beam with 42 μm diameter, Eq. 2.3 provides an effective waist of 14.9 μm, which reduces to a weighted mean $w_e = 10.4$ μm during soliton propagation; this last value is used in Eq. 3.4. The proper use of the effective

waist into Eq. 3.4 accounts for the modal content of the propagating soliton. The theoretical curve fits well to experimental and numerical data at the optimal soliton energy of 1 nJ; for higher or smaller energies, theory and experiment differ significantly, confirming that the soliton theory, Eq. 3.4, only fits at a specific optimal pulse energy.

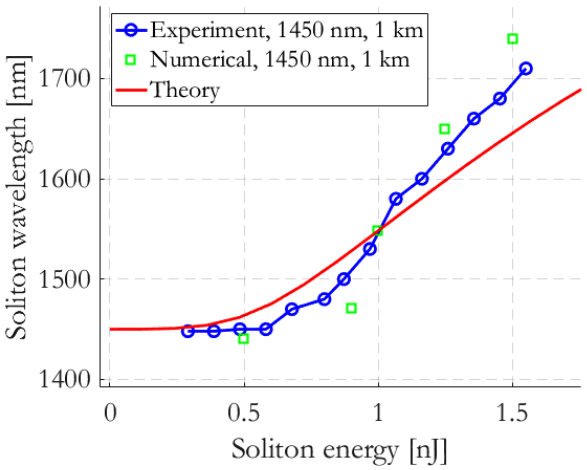

Fig. 4 – Experimental and numerical Raman-induced wavelength shift after 1 km of GRIN fiber, vs. soliton pulse energy, for input pulse with 1450 nm wavelength, 42 μm beam diameter, 60 fs pulsewidth. Red curve is calculated from the theory of Eq. 3.4.

The overall pulse delay induced by Raman SSFS over a distance z is $t_R = |\beta_2|\Delta\omega z$. In order to account for wavelength, dispersion and pulsewidth changes, the time delay must be calculated in differential terms; when expressed in terms of the soliton wavelength shift, we obtain

$$\frac{dt_R}{dz} = D(\lambda)d\Delta\lambda \quad . \qquad (3.5)$$

Fig. 5 shows the experimental delay (blue circles) after 1 km of distance, measured on the oscilloscope traces as the time separation between the leading tail of the dispersive pulse and the top portion of the soliton pulse; the delay was averaged over 3000 consecutive traces. Green squares are obtained from numerical simulations, and the theoretical red curve is calculated by integration of Eqs. 3.5 and 3.4.

Experimental and numerical data are in good agreement, providing a delay of 4800 ps at 1.5 nJ pulse energy, and 1200 ps at the optimal soliton energy of 1 nJ. Also in this case, the theoretical red curve is in best agreement with experimental data at the optimal soliton energy; whereas greater discrepancies are observed for smaller or larger energies.

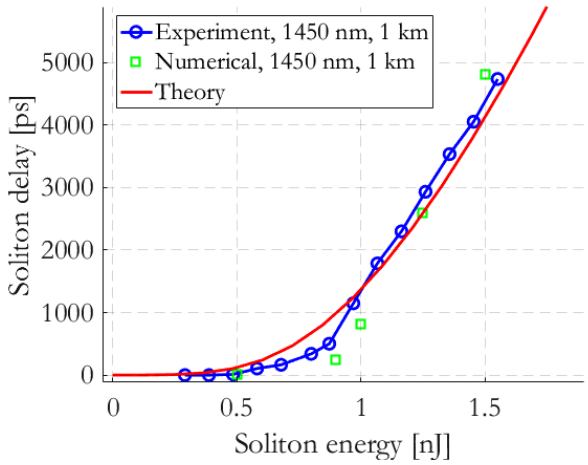

Fig. 5 – Experimental and numerical Raman-induced pulse delay after 1 km of GRIN fiber, vs. soliton pulse energy, for an input pulse with 1450 nm wavelength, 42 μm beam diameter, 60 fs pulsewidth. Red curve is calculated from Eq. 3.5.

B. Statistics of SSFS

By inspecting the output pulses using the fast photodiode, a short soliton pulse was found to delay in time respect to a large, nanosecond dispersive pulse (see Fig. 3b). From the oscilloscope traces, the delay of the peak of the soliton, with respect to the leading tail of the dispersive pulse, was measured; traces show the presence of significant fluctuations, both for the delay and for the peak of the Raman soliton, whose statistics were recorded by relying on sequences of 3000 traces.

Fig. 6 reports the statistics of the SSFS for different soliton energies, as indicated by the values near the individual curves. After an initial increase of the delay jitter, for energies above 1.2 nJ the distributions tend to show a constant standard deviation. To the contrary, the amplitude noise distribution keeps broadening for increasing pulse energy (not shown here). By fitting the delay distributions curves around the soliton energy, we find that the SSFS time jitter is well described by a Gaussian distribution, as it is shown by the dashed red fit for the curve at 1.26 nJ pulse energy. Jitter standard deviation increases from 0.031 to 0.25 ns for energy growing from 0.8 to 1.26 nJ, but then it remains limited to 0.28 ns for energy increasing to 1.55 nJ. The observed SSFS jitter for increasing energy could be motivated by the peak power fluctuations, giving rise to changes in the incremental wavelength shift, Eq. 3.4, and the delay, Eq. 3.5. According to this interpretation, the jitter saturation is explained by the reduction of the incremental wavelength shift with the eight power of the increasing wavelength.

Gordon-Haus interaction between the soliton and the spontaneous Raman noise [31-33] has variance given by $\sigma_t^2 = n_{sp}h\nu\beta_2^2L^2\ln(G)/(3T_0^2E_s)$, with n_{sp} the spontaneous emission factor, G and L the fiber gain and length, respectively. According to this expression, the induced time jitter should be limited to less than 0.2 ps at the energy levels of Fig. 6; hence, Gordon-Haus effect is not sufficient to explain the jitter

observed in the figure, whose standard deviation reaches 280 ps at 1.55 nJ energy, after 1 km distance.

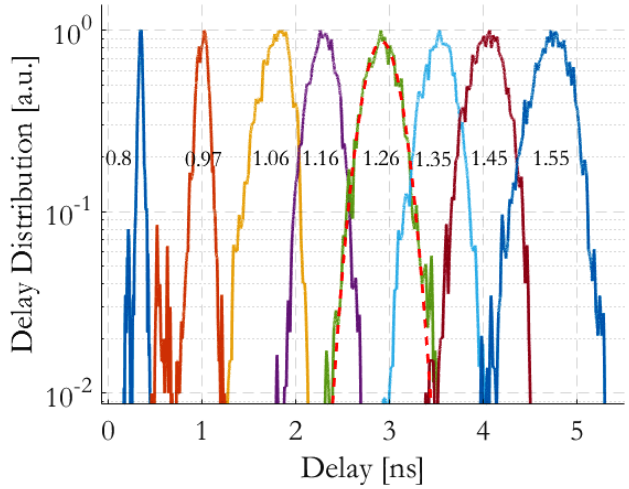

Fig. 6 – Measured statistics for the soliton delay jitter, respect to the residual pulse, at 1 km distance. Numbers near the distribution curves indicate the corresponding soliton energy. The red dashed curve is a Gaussian fit.

IV. Conclusions

Multimode solitons in GRIN fibers show unique properties of pulsewidth and energy invariance, that distinguish them from the properties of well-known single-mode fiber solitons. With the help of numerical simulations and experimental results, we have shown that long-distance multimode solitons are mostly stable at specific energies, and assume precise pulsewidth values, which only depend on the input wavelength. We have shown that the values of pulsewidth and optimal energy can be predicted in terms of the walk-off theory. Based on this result, a SSFS theory accounting for pulse broadening, energy loss, and wavelength-dependence of fiber dispersion and losses, was proposed and compared with experimental results obtained after 1 km of propagation in a GRIN fiber. Our results show a good correspondence with theoretical predictions, both in terms of wavelength red-shift and pulse delay, but only in correspondence of the optimal energy where the MM soliton exhibits a long-range stability. In addition, we demonstrated that multimode solitons, due to their property of forming with a fixed sub-picosecond pulsewidth, are always accompanied by SSFS; this may appear detrimental, to a first sight, for soliton transmission in spatial-division multiplexed transmission systems (SDM). Conversely, the impossibility of forming multimode solitons with picosecond durations can be advantageously used in SDM systems, by launching the proper amount of energy in each degenerate modal group; as we shall discuss in a separate publication, this permits the generation of multiple independent solitons, one for each group, whose stability is not subject to the restrictions of the walk-off theory.

Finally, we discussed how the MM soliton Raman delay is affected by fluctuations, whose statistics were studied experimentally. The soliton jitter, in particular, tends to stabilize for increasing pulse energies, and its statistics can be represented by a Gaussian distribution.

Acknowledgment

We thank Logan Wright et al. for making freely available the open-source parallel numerical mode solver for the coupled-mode nonlinear Schrödinger equations [18]. A modified version of the code was used for this work.

References

1. A. Hasegawa, “Self-confinement of multimode optical pulse in a glass fiber,” Opt. Lett. 5, pp. 416–417 (1980).
2. Y. Silberberg, “Collapse of optical pulses,” Opt. Lett. 15, pp. 1282–1284 (1990).
3. D. J. Richardson, J. M. Fini, L. E. Nelson, “Space-division multiplexing in optical fibers,” Nat. Phot. 7, 2013.94 (2013).
4. L. G. Wright, D. N. Christodoulides, F. W.Wise, “Spatiotemporal mode-locking in multimode fiber lasers,” Science 358, pp. 94–97 (2017).
5. W. H. Renninger, F. W. Wise, “Optical solitons in graded-index multimode fibres,” Nat. Comm. 4:1719, DOI: 10.1038/ncomms2739 (2013).
6. L. G. Wright, W. H. Renninger, D. N. Christodoulides, F. W. Wise, “Spatiotemporal dynamics of multimode optical solitons,” Opt. Expr. 23(3), pp. 3492-3506 (2015).
7. Z. Zhu, L. G. Wright, D. N. Christodoulides, F. W. Wise, “Observation of multimode solitons in few-mode fibers,” Opt. Lett. 41(20), pp. 4819-4822 (2016).
8. K. Krupa, A. Tonello, A. Barthélémy, T. Mansuryan, V. Couderc, G. Millot, P. Grelu, D. Modotto, S. A. Babin, and S. Wabnitz, “Multimode nonlinear fiber optics, a spatiotemporal avenue,” APL Photonics 4(11), 110901 (2019).
9. A. Picozzi, G. Millot, S. Wabnitz, “Nonlinear virtues of multimode fibre,”. Nature Photon 9, pp. 289–291 (2015). https://doi.org/10.1038/nphoton.2015.67
10. F. M. Mitschke, L. F. Mollenauer, “Discovery of the soliton self-frequency shift,” Opt. Lett. 11(10), pp. 659–661 (1986).
11. J. P. Gordon, “Theory of the soliton self-frequency shift,” Opt. Lett. 11(10), Oct. 1986.
12. A. B. Grudinin, E. M. Dianov, D. V. Korbkin, A. M. Prokhorov, D. V. Khaidarov, “Nonlinear mode coupling in multimode optical fibers; excitation of femtosecond-range stimulated-Raman-scattering solitons,” JEPT Lett. 47(6), pp. 356-359 (1988).
13. K. J. Blow, N. J. Doran, D. Wood, “Suppression of the soliton self-frequency shift by bandwidth-limited amplification,” J. Opt. Soc. Am. B 5(6), pp. 1301-1304 (1988).
14. J. Santhanam, G. P. Agrawal, “Raman-induced spectral shift in optical fibers: general theory based on the moment method,” Opt. Comm. 222, pp. 413-420 (2003).
15. U. Bandelow, S. Amiranashvili, S. Pickartz, “Stabilization of optical pulse transmission by exploiting fiber nonlinearities,” JLT 38(20),pp. 5743-5747 (2020).
16. M. Zitelli, F. Mangini, M. Ferraro, O. Sidelnikov, and S. Wabnitz, “Conditions for walk-off soliton generation in a multimode fiber,” Commun. Phys. 4(1), 182 (2021).
17. P. J. F. Poletti, and P. Horak, "Description of ultrashort pulse propagation in multimode optical fibers," J. Opt. Soc. Am. B 25, 1645 (2008).
18. L. G. Wright, Z. M. Ziegler, P. M. Lushnikov, Z. Zhu, M. A. Eftekhar, D. N. Christodoulides, and F. W. Wise, "Multimode nonlinear fiber optics: massively parallel numerical solver, tutorial, and outlook," IEEE J. Sel. Top. Quantum Electron. 24, 1-16 (2018).
19. S. Mumtaz, R. J. Essiambre, G. P. Agrawal, “Nonlinear propagation in multimode and multicore fibers: generalization of the Manakov equations,” JLT 31(3), pp. 398-406 (2013).
20. A. Mecozzi, C. Antonelli, and M. Shtaif, “Coupled Manakov equations in multimode fibers with strongly coupled groups of modes,” Opt. Express 20, pp. 23436–23441 (2012).
21. R. H. Stolen, J. P. Gordon, W. J. Tomlinson, and H. A. Haus, “Raman response function of silica-core fibers,” J. Opt. Soc. Am. B 6, 1159–1166 (1989).
22. G. P. Agrawal, Nonlinear Fiber Optics, 3rd ed. (Academic, 2001).
23. J. T. Manassah, P. L. Baldeck, R. R. Alfano, “Self-focusing and self-phase modulation in a parabolic graded-index optical fiber,” Opt. Lett. 13(7), pp. 589-591 (1988).

24. M. Karlsson, D. Anderson, M. Desaix, "Dynamics of self-focusing and self-phase modulation in a parabolic index optical fiber," Opt. Lett 17(1), pp. 22-24 (1992)
25. T. Hansson, A. Tonello, T. Mansuryan, F. Mangini, M. Zitelli, M. Ferraro, A. Niang, R. Crescenzi, S. Wabnitz, V. Couderc, "Nonlinear beam self-imaging and self-focusing dynamics in a GRIN multimode optical fiber: theory and experiments," Opt. Expr. 28(16), pp. 24005-24021.
26. F. Mangini, M. Ferraro, M. Zitelli, A. Niang, A. Tonello, V. Couderc, O. Sidelnikov, F. Frezza, S. Wabnitz, "Experimental observation of self-imaging in SMF-28 optical fibers," Opt. Expr. 29(8), pp. 12625-12633 (2021).
27. M. Zitelli, Y. Sun, M. Ferraro, F. Mangini, O. Sidelnikov, V. Couderc, S. Wabnitz, "Multimode solitons in step-index fibers," Opt. Expr. 30(4), pp. 6300-6310 (2022).
28. M. Zitelli, M. Ferraro, F. Mangini, and S. Wabnitz, "Single-mode spatiotemporal soliton attractor in multimode GRIN fibers," Photonics Res. 9(5), 741–748 (2021).
29. M. A. Eftekhar, H. Lopez-Aviles, F. W. Wise, R. Amezcua-Correa, D. N. Christodoulides, "General theory and observation of Cherenkov radiation induced by multimode solitons," Comm. Phys. 4:137 (2021).
30. A. S. Ahsan, G. P. Agrawal, "Spatio-temporal enhancement of Raman-induced frequency shifts in graded-index multimode fibers," Opt. Lett 44(11), pp. 2637-2640 (2019).
31. J. P. Gordon, H. A. Haus, "Random walk of coherently amplified solitons in optical fiber transmission," Opt. Lett. 11(19), pp. 665-667 (1986).
32. S. Wabnitz, Undersea Fiber Communication Systems, ch.8 (Academic, 2002).
33. C. J. McKinstrie, J. Santhanam, G. P. Agrawal, "Gordon–Haus timing jitter in dispersion-managed systems with lumped amplification: analytical approach," J. Opt. Soc. Am. B 19(4), pp. 640-649 (2002).

Mario Zitelli obtained the M.Sc. in Electronics Engineering and the Ph.D. in Applied Electromagnetism from Sapienza University of Rome in 1995 and 1999 respectively. From 1997 to 1999 he was with Ugo Bordoni Foundation (FUB); since 1999 he has worked as a senior researcher and R&D manager in several telecom companies: Pirelli Submarine Telecom Systems (Milan, Italy), QPlus Networks Inc. (Long Beach, CA), Santel Networks Inc. (Fremont, CA), CNET France-Telecom (Lannion, France), TelCon (Rome, Italy), OCEM Airfield Technology (Valsamoggia, Italy), Leonardo (Pomezia, Italy), Selex System Integrations (Overland Park, Kansas, USA), Argos Ingegneria (Rome, Italy), Photoneco ltd (London, UK). Since July 2019 he is researcher in Telecommunications at Sapienza University of Rome. His research activities include nonlinear fiber transmission, spatio-temporal nonlinear effects, advanced optical modulation formats, photometry. He is author/co-author of over 60 international refereed papers and conference presentations, 6 international patents, and was member/co-director of 5 research projects from EU, NATO, FILAS.

Mario Ferraro received the Bachelor's degree in Physics "cum laude and special mention to the curriculum" in 2013 from University of Calabria (Italy) and the Master degree in Physics "cum laude" in 2015 from "La Sapienza" University of Rome (Italy). He has been awarded as excellent graduated student of "La Sapienza" University of Rome in 2016 and he received the Ph.D. in Physics in 2019 from the University of Côte d'Azur in Nice (France). His research activity has concerned nonlinear optics in nanodisordered media as well as semiconductor-based hyperbolic metameterials. Since January 2020 he is a postdoctoral fellow at the Engineering department of "La Sapienza" University of Rome working on ultrafast nonlinear phenomena in multimode optical fibers.

Fabio Mangini received his B.Sc. in Clinical Engineering and M.Sc. in Biomedical Engineering "cum laude" from "La Sapienza" University of Rome, Italy in 2005 and 2008, respectively. He earned his Ph.D. in Electromagnetism from the Department of Information Engineering, Electronics, and Telecommunications of the same University in 2014. In June 2014 and in May 2015, he won the "Young Scientist Award" from URSI (International Union of Radio Science). In January 2017, he won the "Ph.D. ITalents" prize and in October 2018 he won the "Marabelli prize". Between 2009 and 2015 he worked at the Laboratory of Electromagnetic Fields II at "La Sapienza" University of Rome. His research activities focus on guiding structures, numerical methods, theoretical scattering models, optical propagation, anisotropic media, metamaterials, biomedical applications, and cultural-heritage applications. Since April 2019, he has been working, as a researcher, at the Electromagnetic Fields and Photonics group at the University of Brescia.

Stefan Wabnitz obtained the Laurea Degree in Electronics Engineering from Sapienza University of Rome in 1982, the MS in Electrical Engineering from Caltech in 1983, and the PhD in Applied Electromagnetism from the Italian Ministry of Education in 1988.

He was with the Ugo Bordoni Foundation between 1985 and 1996. From 1996 until 2007 he was full professor at the University of Burgundy in Dijon, France. Between 1999 and 2003 he was with Alcatel Research and Innovation Labs in France, and with Xtera Communications in Allen, Texas, USA. Since 2007 until 2018 he was full professor in Electromagnetic Fields at the University of Brescia, Italy. Since November 2018 he is full professor in Telecommunications at Sapienza University of Rome. His research activities involve nonlinear propagation effects in optical communications and information processing devices.

Prof. Wabnitz is the author and co-author of over 800 international refereed papers, conference presentations, and book chapters. He is the Editor-in-Chief of Elsevier's Optical Fiber Technology, a Fellow member of the Optical Society of America, and senior member of IEEE-Photonics Society.